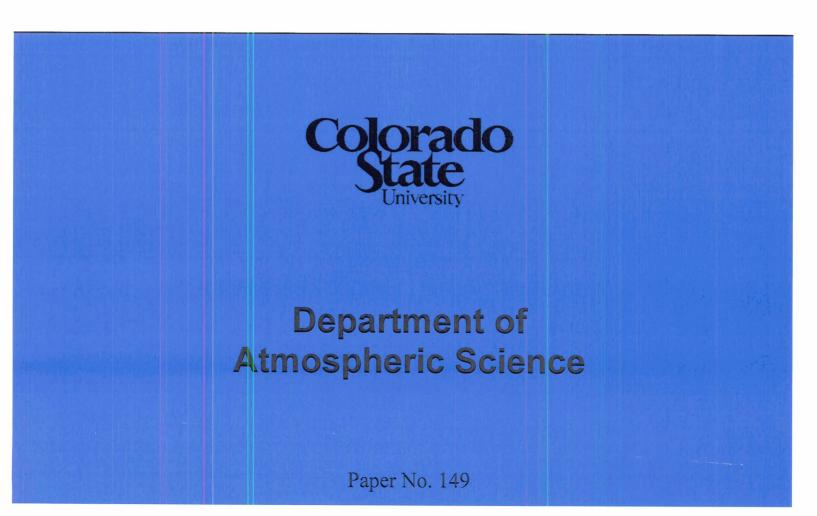# Eddy Processes in Momentum Transport and Kinetic Energy Distribution

By
E.R. Reiter and M.E. Glasser

Department of Atmospheric Science
Colorado State University
Fort Collins, Colorado

Colorado State University

Department of Atmospheric Science

Paper No. 149

EDDY PROCESSES IN MOMENTUM TRANSPORT AND KINETIC ENERGY DISTRIBUTION[1]

by

E. R. Reiter and M. E. Glasser[2]

2) Department of Atmospheric Science, Colorado State University, Fort Collins, Colorado 80521.

Abstract

Meridional fluxes of angular momentum and kinetic energy values have been computed for the month of January 1964 between the 500 and 100-mb levels and between $30^{O}N$ and $70^{O}N$ for five longitudinal sectors of the Northern Hemisphere. Numerical values of these quantities are presented for combinations of barotropic, baroclinic, standing, transient, mean meridional and eddy flux processes. Comparison of these data with radioactive fallout events supports the results from earlier case studies.

The computational methods outlined here may be applied to other regions of the atmosphere in which vertical and horizontal gradients of atmospheric properties (such as ozone) reveal a marked time variation and are in a significant way transported by synoptic-scale three-dimensional eddies.

1. Introduction

Studies of the energetics of the atmospheric general circulation revealed the important fact that the mean zonal flow is "fed" by eddies of planetary and cyclone scale (for references, see Reiter, 1969a). These eddies, in turn, are maintained by conversion of potential to kinetic energy by the release of baroclinic instability and not so much by a barotropic redistribution of the kinetic energy of the mean flow. This conversion of energy involves vertical mass flux which will produce vertical mixing of atmospheric trace substances, such as radio-active debris. Thus, a better understanding of the eddy processes in energy fluxes and conversions may yield considerable insight into the transport mechanisms of trace constituents of the atmosphere, and vice versa. The present study, therefore, attempts to correlate parameters representative of the energetic processes in the upper troposphere with mass transports at these levels and with radioactive fallout events at the earth's surface. During periods sufficiently removed from atmospheric testing of nuclear devices, radioactive fallout is indicative of the transfer of (contaminated) stratospheric air into the lower troposphere, and hence of strong vertical mass transports in the tropopause region.

In the discussion of <u>mean</u> and <u>eddy</u> terms describing momentum transport and kinetic energy distribution a new notation will be used (Reiter, 1969b) which allows estimates of the various contributions of barotropic, baroclinic, standing and transient flow processes. Computations have been carried out for various longitude sectors of the Northern Hemisphere which correspond to the distribution of continents and oceans. The time period chosen for this investigation, January 1964, was characterized by significant regional fallout events over North America. A blocking anticyclone persisted over western Europe throughout the period (Andrews, 1964; Sawyer, 1965).

2. Data

Geostrophic u and v-components were computed for 5° latitude and longitude grid intervals between 30^ON and 70^ON and at the 500, 400, 300, 200, and 100-mb levels. The wind components were evaluated by a space-centered finite difference technique using height fields analyzed by the Air Force, Global Weather Central, Offutt AFB, Omaha, Nebraska. The height data were originally available on the National Meteorological Center octagonal grid, and were transferred to the 5° latitude-longitude grid by means of a 16-point Bessel interpolation scheme. (For an objective analysis of the "raw" height data, see Murray, 1963.)

The wind data thus obtained were treated separately by longitudinal sectors. These are defined in Table 1, and comprise 70° of longitude each. It should be noted here that sectors NA and AO show a 20° long. overlap, whereas a gap of 15° long. appears between sectors AO and E, and another one of 15° long. between sectors PO and NA. The sector-wise treatment of the data was in part dictated by necessity, since data storage for longitude $0^O \leq \lambda \leq 360^O$, latitude 30^ON $\leq \phi \leq 70^O$N, pressure 100 mb $\leq p \leq$ 500 mb and time 1 January 1964 $\leq t \leq$ 30 January 1964, at increments $\Delta\lambda = 5^O$, $\Delta\phi = 5^O$, Δp = 100 mb, and Δt = 24 hours (using 1200 GMT data), would have exceeded the memory capacity of the CDC 6400 on which the computations were performed. Computation by sector offered the advantage that at least a limited insight could be gained into the behavior of momentum transports and kinetic energy in the wave-number space for n < 5, in addition to their treatment in the λ, ϕ, p, t spaces.

TABLE 1: Geographical sectors used in determining
the regional distribution of momentum
transports and kinetic energies.

Geographic Region	Sector Designation	Longitudinal Range
North America	NA	$130^{\circ}W - 60^{\circ}W$
Atlantic Ocean	AO	$80^{\circ}W - 10^{\circ}W$
Europe	E	$5^{\circ}E - 75^{\circ}E$
Asia	A	$75^{\circ}E - 145^{\circ}E$
Pacific Ocean	PO	$145^{\circ}E - 145^{\circ}W$

3. Averaging Procedure

In the following section the eddy breakdown technique commonly used in meteorological investigations is contrasted to a more recent approach introduced by Reiter (1969b). The notation suggested by Reiter (1969b) will be used in the discussion. It indicates averaging processes by brackets and departures from such averages by parentheses. Subscripts in parentheses indicate the coordinates over which the averaging or departure-taking was performed. Thus

$$u = [u]_{(p)} + (u)_{(p)} \tag{1}$$

conforms to the standard Reynolds notation

$$u = \bar{u} + u' \tag{2}$$

where the averages and departures are taken with respect to pressure. Momentum fluxes in this pressure domain yield products of the form

$$uv = [u]_{(p)}[v]_{(p)} + [u]_{(p)}(v)_{(p)} + (u)_{(p)}[v]_{(p)} + (u)_{(p)}(v)_{(p)} \tag{3}$$

which may be averaged over pressure to produce

$$[uv]_{(p)} = [u]_{(p)}[v]_{(p)} + [(u)_{(p)}(v)_{(p)}]_{(p)} \tag{4}$$

(Note that $[[u]_{(p)}]_{(p)} = [u]_{(p)}$ and $[(u)_{(p)}]_{(p)} = 0$.)

Further expansions of expressions of this type generally follow the techniques first introduced by Starr and White (1951). Only the

first term, the term involving the product of mean quantities, is affected by the expansion. It is assumed that

$$[u]_{(p)} = [u]_{(p,\lambda)} + ([u]_{(p)})'_{(\lambda)} \tag{5}$$

with a similar expression for $[v]_{(p)}$. Substitution into Eqn. (4) and averaging over λ yields

$$[uv]_{(p,\lambda)} = [u]_{(p,\lambda)}[v]_{(p,\lambda)} + [([u]_{(p)})'_{(\lambda)}([v]_{(p)})'_{(\lambda)}]_{(\lambda)}$$

$$+ [(u)_{(p)}(v)_{(p)}]_{(p,\lambda)} \quad . \tag{6}$$

To expand Eqn. (6) in the time domain it is assumed that

$$[u]_{(p,\lambda)} = [u]_{(p,\lambda,t)} + ([u]_{(p,\lambda)})'_{(t)} \tag{7}$$

with a similar expression for $[v]_{(p,t)}$. Substitution into Eqn. (6) and averaging over t yields

$$[uv]_{(p,\lambda,t)} = [u]_{(p,\lambda,t)}[v]_{(p,\lambda,t)}$$

$$+ [([u]_{(p,\lambda)})'_{(t)}([v]_{(p,\lambda)})'_{(t)}]_{(t)}$$

$$+ [([u]_{(p)})'_{(\lambda)}([v]_{(p)})'_{(\lambda)}]_{(\lambda,t)}$$

$$+ [(u)_{(p)}(v)_{(p)}]_{(p,\lambda,t)} \quad . \tag{8}$$

Jensen (1961) used this expression for an expansion of the product ωt with the coordinates t, λ and ϕ. Other expressions over 3 or 4 variables (e. g. , Barnes, 1962; Oort, 1964) follow the same pattern set by Starr and White (1951).

For a less restrictive development Reiter (1969b) applies the following substitutions in place of the assumptions used in Eqns. (5) and (7),

$$u = [u]_{(\lambda)} + (u)_{(\lambda)} \tag{9}$$

and

$$u = [u]_{(t)} + (u)_{(t)} \; . \tag{10}$$

To obtain an expression similar to Eqn. (8) the order of substitution is reversed. In Starr's and White's method the deviations initially introduced remain unaltered throughout the development while in Reiter's expansion subsequent substitutions affect each term. The result is Eqn. (11) which now contains 8 terms, each carrying its own significance as to barotropic, baroclinic, standing, transient, mean meridional and eddy transports (see Eqn. (21) Reiter, 1969b).

$$[uv]_{(p, \lambda, t)} = [u]_{(p, \lambda, t)} [v]_{(p, \lambda, t)}$$

    ① barotropic standing mean meridional

$$+ \; [[(u)_{(p)}]_{(\lambda, t)} [(v)_{(p)}]_{(\lambda, t)}]_{(p)}$$

    ② baroclinic standing mean meridional

$$+ \; [[([u]_{(p)})_{(\lambda)}]_{(t)} [([v]_{(p)})_{(\lambda)}]_{(t)}]_{(\lambda)}$$

    ③ barotropic standing eddy

$$+ \left[\left[(u)_{(p,\lambda)}\right]_{(t)}\left[(v)_{(p,\lambda)}\right]_{(t)}\right]_{(p,\lambda)}$$ ④ baroclinic standing eddy

$$+ \left[\left([u]_{(p,\lambda)}\right)'_{(t)}\left([v]_{(p,\lambda)}\right)'_{(t)}\right]_{(t)}$$ ⑤ barotropic transient mean meridional

$$+ \left[\left(\left[(u)_{(p)}\right]_{(\lambda)}\right)'_{(t)}\left(\left[(v)_{(p)}\right]_{(\lambda)}\right)'_{(t)}\right]_{(p,\,t)}$$ ⑥ baroclinic transient mean meridional

$$+ \left[\left([u]_{(p)}\right)'_{(\lambda,\,t)}\left([v]_{(p)}\right)'_{(\lambda,\,t)}\right]_{(\lambda,\,t)}$$ ⑦ barotropic transient eddy

$$+ \left[(u)_{(p,\,\lambda,\,t)}(v)_{(p,\,\lambda,\,t)}\right]_{(p,\,\lambda,\,t)}$$ ⑧ baroclinic transient eddy

(11)

In the actual computations, whose results will be shown later, a factor of $\cos\phi$ was applied to the longitudinal segments in order to account for the convergence of meridians. Since ϕ did not enter into the averaging process one may write

$$[uv\cos\phi]_{(p,\lambda,t)} = \cos\phi\ [uv]_{(p,\lambda,t)} . \tag{12}$$

For the sake of convenience this factor of $\cos\phi$ has not been shown in Eqn. (11).

4.   Comparison of Computational Techniques

A numerical comparison was made between the terms appearing in Eqn. (11) (after Reiter) and those in Eqn. (8) (after Starr and White). The barotropic standing mean meridional and barotropic transient mean meridional terms (① and ⑤) of Eqn. (11) are also common to Eqn. (8). As would be expected, the sum of the terms remaining in Eqn. (11) (② , ③ , ④ , ⑥ , ⑦ and ⑧) exactly equaled the sum of the terms remaining in Eqn. (8) (the second and fourth terms).

$[(u)_{(p)}(v)_{(p)}]_{(p, \lambda, t)}$ contains the only baroclinic contribution in Eqn. (8). Equivalence of the baroclinic contributions (② , ④ , ⑥ and ⑧) in Eqn. (11) was tested for both u^2 and v^2 at each latitude in each sector. In every case the baroclinic contribution from Reiter's formulation was nearly equal to, but slightly larger than, the baroclinic contribution of Starr's and White's formulation. For u^2 this difference amounted to 3 per cent on the average for the entire hemisphere. The difference at latitudes 30 to 35°N, where the u^2 baroclinic contributions were largest, was 1 per cent or less. For v^2 the difference was somewhat larger, amounting to an average of 7 per cent for the entire hemisphere. The smallest percentage differences in the computation of v^2 were in the lower latitudes where the baroclinic effects for v^2 are small. Since the baroclinic contributions from Reiter's method are in all cases larger than from Starr's and White's method, the use of a larger data sample is not expected to reduce the difference between the two computational methods.

It follows from the foregoing that the remaining second term of Eqn. (8) is equivalent to the sum of the barotropic standing eddy and the barotropic transient eddy terms of Eqn. (11) (terms ③ and ⑦). Table 2 shows the equivalence that has been established between the two methods of eddy computations. The effect of the more restrictive

assumptions by Starr and White is to combine the transient, standing, eddy and mean meridional contributions of the baroclinic motion into one term, and the standing and transient contributions of the barotropic eddy into another term. The computational technique developed by Reiter gives more detailed information on the characteristics of the atmospheric circulation.

TABLE 2: The terms in the eddy breakdown of a variable over three coordinates.

(After Starr and White (Eqn. (8)) and after Reiter (Eqn. (11)))

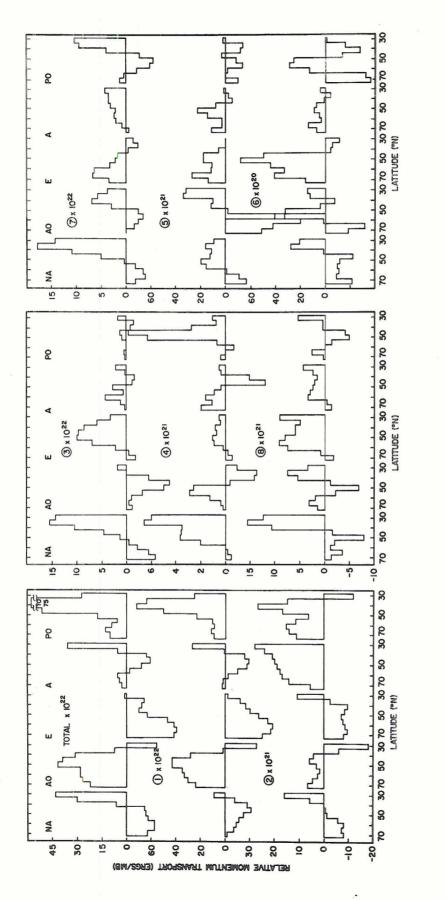| Eqn. (8), Starr and White	Equivalence Between Terms	Eqn. (11), Reiter
$[u]_{(p,\lambda,t)}[v]_{(p,\lambda,t)}$	barotropic standing mean-meridional	① $[u]_{(p,\lambda,t)}[v]_{(p,\lambda,t)}$
$[([u]_{(p)}'_{(\lambda)}[v]_{(p)}'_{(\lambda)})]_{(\lambda,t)}$	barotropic eddy $\Big\{$ standing / transient	③ $[[([u]_{(p)}'_{(\lambda)}]_{(t)}[[v]_{(p)}'_{(\lambda)}]_{(t)}]_{(\lambda)}$
		⑦ $[([u]_{(p)}'_{(\lambda,t)}[v]_{(p)}'_{(\lambda,t)}]_{(\lambda,t)}$
$[([u]_{(p,\lambda)}'_{(t)}[v]_{(p,\lambda)}'_{(t)})]_{(t)}$	barotropic transient mean-meridional	⑤ $[[u]_{(p,\lambda)}'_{(t)}[v]_{(p,\lambda)}'_{(t)}]_{(t)}$
$[(u)_{p)}(v)_{(p)}]_{(p,\lambda,t)}$	baroclinic $\Big\{$ standing mean-meridional / standing eddy / transient mean meridional / transient eddy	② $[[(u)_{(p)}]_{(\lambda,t)}[(v)_{(p)}]_{(\lambda,t)}]_{(p)}$
		④ $[[(u)_{(p,\lambda)}]_{(t)}[(v)_{(p,\lambda)}]_{(t)}]_{(p,\lambda)}$
		⑥ $[([(u)_{(p)}]_{(\lambda)}'_{(t)}([(v)_{(p)}]_{(\lambda)}'_{(t)}]_{(p,t)}$
		⑧ $[(u)_{(p,\lambda,t)}(v)_{(p,\lambda,t)}]_{(p,\lambda,t)}$

5. Results of Momentum Transport Computations

Fig. 1 shows an evaluation of all terms contained in Eqn. (11). [Note that different scales have been used in the presentation of various terms. The numbers in circles refer to the numbers of the terms as they appear in Eqn. (11).] Results are given for the individual longitudinal sectors described in Table 1, and for latitude circles at 5° intervals between 30°N and 70°N.
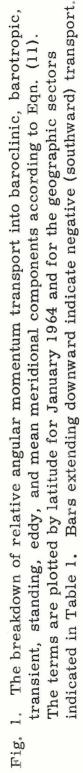
In Fig. 2 the data from Fig. 1 has been arranged by plotting the longitudinal averages of the various terms in Eqn. (11) at 30°N, 50°N and 70°N for each sector. These averages are plotted longitude-wise at the center of each sector. Smooth curves were drawn through the data points, giving a crude indication of the behavior of the individual terms in wave-number space for $n < 5$.

It appears that the Pacific sector carried the bulk of northward momentum transport mainly at low and middle latitudes, followed by the Atlantic sector. Over Europe, where a blocking high had established itself, southward momentum transport prevailed (Fig. 1, "Total"). Only term ① (barotropic standing mean meridional flow), term ③ (barotropic standing eddy) and term ⑦ (barotropic transient eddy) achieved significant contributions towards the total transport. Term ⑥ (baroclinic transient mean meridional flow) may be neglected altogether.

It should be pointed out that the "mean meridional circulation" of term ① refers to sector averages. Had hemispheric averages been taken, a large fraction of this term would probably shift towards a contribution from "barotropic standing eddies" (term ③). This may be gathered from Fig. 2 which indicates that the individual sector

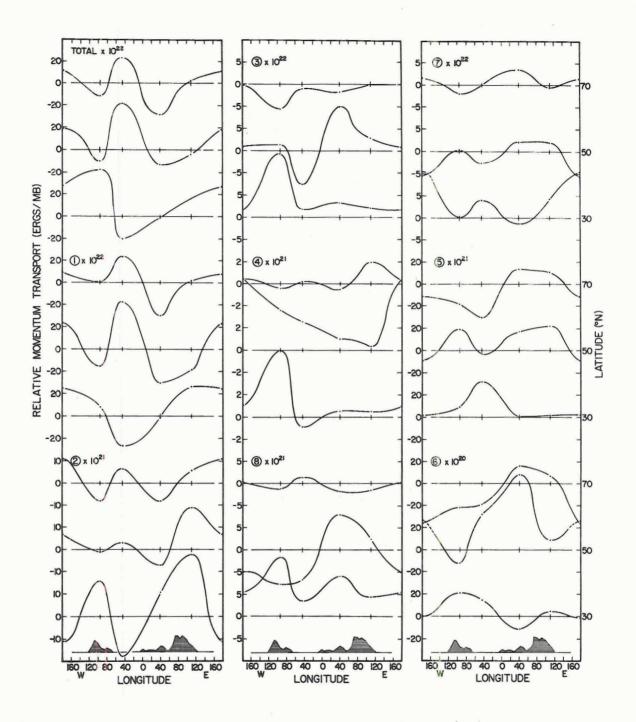Fig. 1. The breakdown of relative angular momentum transport into baroclinic, barotropic, transient, standing, eddy, and mean meridional components according to Eqn. (11). The terms are plotted by latitude for January 1964 and for the geographic sectors indicated in Table 1. Bars extending downward indicate negative (southward) transport.

Fig. 2. Relative angular momentum transport for each of the terms of Eqn. (11). These values, representing longitudinal averages over each sector at 30°N, 50°N, and 70°N, are taken from Fig. 1 and are plotted at the center of each sector. Negative values indicate southward transport.

averages of term ① contribute in a two-wave pattern at middle and high latitudes, and in a one-wave pattern at low latitudes. These results are in agreement with computations by Miller et al. (1967) for time-averaged angular momentum transport as a function of wave number. The 500-mb geostrophic angular momentum transport averaged over a ten-year period showed that equatorward transport by wave number 2 at high latitudes extends further south, and is much larger in magnitude, than the transport by any of the other wave numbers. A maximum poleward momentum transport in wave number 1 was found by Miller et al. to occur in winter near 35^ON. The "total transport" shown in Fig. 2 also reveals a transport by wave number 1 at 30^ON. It has been found by other investigators that these low wave numbers usually characterize standing planetary waves. (For references, see Reiter, 1963a, 1969a.)

Momentum transports by the "baroclinic" portions of the current, i. e., by the contributions of vertical wind shears between 500 and 100 mb in mean and eddy flow patterns (terms ② , ④ , ⑥ and ⑧) are considerably smaller than those accomplished by the "barotropic" (i. e., vertically averaged) portion of the current (terms ① , ③ , ⑤ and ⑦). Among the baroclinic terms, ② (baroclinic standing mean meridional flow) is the most prominent, especially in the Asian and Pacific sectors. This may be attributed to the sharply shearing jet streams which appear over these regions during the winter season. In Fig. 2 at 30^ON we find that term ② indicates very sharp poleward momentum flux over Asia and somewhat less flux over North America. In actuality these fluxes tend to occur mainly in the vicinity of Japan and near the eastern seaboard of the United States, i. e., close to the eastern borders of the geographical sectors given in Table 1. These fluxes dominate the sector average which, when plotted at the

geographic mid-point of the sector (as has been done in Fig. 2), makes the strong southwesterly flow appear to occur farther to the west then it does in reality.

Details of the momentum flux configuration over sector NA (North America) are shown in Fig. 3. The upper portion of this diagram gives a time-latitude section of the meridional flux of zonal momentum averaged vertically over $100 \leq p \leq 500$ mb and zonally over $60^{\circ}W \leq \lambda \leq 130^{\circ}$ W. The diagram in the center of Fig. 3 gives "momentum flux convergence" computed as the difference of momentum flux over 5° latitude intervals (negative values represent divergence). The bottom diagram shows the zonal wind component averaged vertically and zonally over the same pressure and longitude ranges. The existing, but poor, correlation between the center and lower diagrams indicates that momentum flux convergence in a limited geographic sector is one--but by no means the only--mechanism by which the genesis and maintenance of jet streams may be explained.
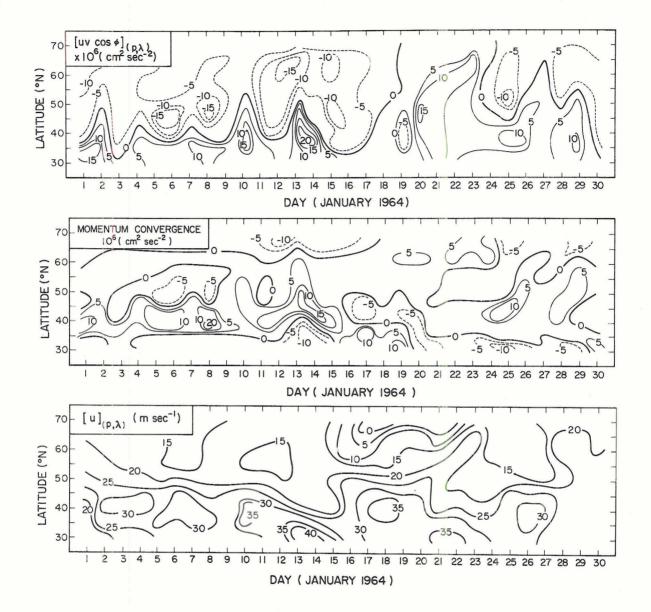
Fig. 3. Latitude-time section of relative angular momentum transport (upper diagram) for the middle latitude upper troposphere over the North American sector. Negative values indicate southward transport. Middle diagram: Momentum convergence and divergence in relative units as computed from the upper figure. Negative values indicate divergence. Lower diagram: Latitude-time section of zonal velocity for the middle latitude upper troposphere over the North American sector.

6. Momentum Transport and Radioactive Fallout

The upper portion of Fig. 3, which shows strong surges of momentum flux in the upper troposphere and lower stratosphere may be correlated with radioactive fallout events. The latter are shown in the bottom diagram of Fig. 4 in terms of longitudinally averaged β-activity plotted as a function of latitude and time. The plot on the right side of this diagram contains the latitudinal monthly-mean fallout distribution over North America during January 1964. From earlier investigations Danielsen, 1959; Mahlman, 1964, 1965, 1966; Reiter and Mahlman, 1964, 1965) it appears that cyclogenetic activity near tropopause level leads to intrusion of stratospheric air into the troposphere. These intrusions, leading to surface fallout, occur mainly within the stable region of the "jet stream front" (Danielsen, 1964; Reiter, Glasser and Mahlman, 1967, 1969).

As one means of estimating cyclogenetic events we may use the momentum flux data shown in Fig. 3. Strong southward transports-- which from synoptic experience are usually associated with sinking motions in the upper troposphere--occur in middle and high latitudes on the dates given in Table 3. Corresponding fallout events are listed in the same table.

It appears that a lag of approximately two days occurs most frequently between southward surges of westerly momentum and surface fallout. This is in good agreement with case studies of radioactive debris trajectories (e. g. , Reiter and Mahlman, 1964). A comparison between Figs. 3 and 4 reveals furthermore that mid-latitude cyclogenetic activity usually tends to well-pronounced fallout events over the southern United States. This fact has also been corroborated by several synoptic case studies (Reiter, 1963b; Reiter and
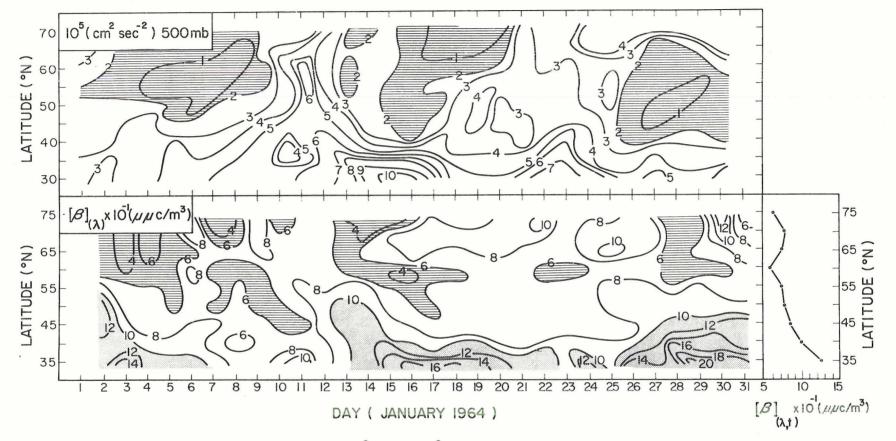
Fig. 4. Latitude-time section of $\{(u)^2_{(p)} + (v)^2_{(p)}\}/2$ (upper diagram) for the 500 mb surface over the North American sector during January 1964. Minima are represented by horizontal hatching. Latitude-time section of the surface air β activity (lower diagram) averaged over a longitude range from 75°W to 125°W for January 1964. Minima are represented by horizontal hatching and maxima are stippled. The time average (January 1964) of the lower figure is given on the right.

TABLE 3: Comparison of momentum flux surges and
surface fallout events over North America.

Observation	Dates, January 1964						
Southward Momentum Flux, Mid-latitudes	< 1	6	8	12	15	19	25
Surface Fallout < 60 N	2-3	8	10-11	14-22		24	26 -
Southward Momentum Flux, High Latitudes			(7)	12	15	25	28
Surface Fallout > 60 N			9	15 -	22 - 27	30 -	

Mahlman, 1964, 1965). The secondary fallout maximum over Canada
(small diagram, right lower portion of Fig. 4) is associated with dis-
turbances traveling north of the United States border. The Arctic
front jet stream, thus, appears to cause stratospheric-tropospheric
mass exchange processes very similar to those brought about by the
polar-front jet. To the authors' knowledge no case studies or magni-
tude estimates of stratospheric-tropospheric mass exchange processes
are available as yet for jet streams in the Arctic and sub-Arctic regions.
From Figs. 3 and 4 it appears that such flux processes may have con-
siderable magnitudes. They should be directed downward as well as
upward, the latter importing tropospheric air into the stratosphere.
Since the tropopause lies at relatively high pressures and temperatures
in the polar region, it is conceivable that the return-flow of tropospheric
air into the stratosphere might carry aloft measurable amounts of water
vapor. Such a flux would have to be considered in the stratospheric
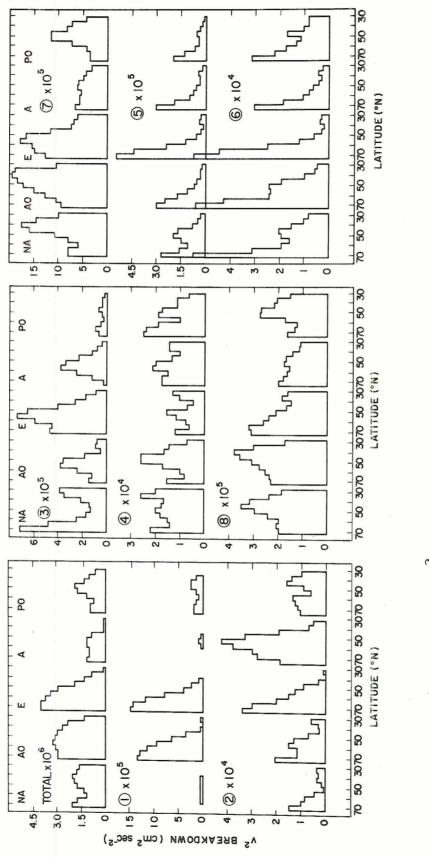water vapor budget.

7. Kinetic Energy

The total u and v-component contributions to specific kinetic energy, $[u^2]_{(p,\lambda,t)}$ and $[v^2]_{(p,\lambda,t)}$, may be expanded in analogy to Eqn. (11) into barotropic, baroclinic, standing, transient, mean meridional and eddy terms. The results of such a computation for January 1964 are shown in Figs. 5 and 6 as a function of latitude and for the individual hemispheric sectors of Table 1. Again it should be pointed out that different scales have been used for the different terms whose numbers in circles correspond to those in Eqn. (11). The energy lies mainly in the "barotropic standing mean meridional u-component" (Fig. 5, term ①). The blocking situation over the Atlantic and European sectors reveals itself mainly in the relatively large amplitudes of term ① for these sectors in the v-component (Fig. 6), especially at high latitudes. Of the baroclinic terms in the v-component of kinetic energy only the transient eddies (term ⑧) give a significant contribution. In the u-component the baroclinic terms ② and ⑧ (standing mean meridional and transient eddy kinetic energies) are of comparable magnitudes. The baroclinic terms in general contribute less than the corresponding barotropic terms as evident from Table 4. This table gives the per-cent contribution of the different classes of "eddies" (baroclinic, transient and stand- ing eddy) to the total kinetic energy of a given sector. These values are determined by averaging each term ① through ⑧ of Figs. 5 and 6 latitudinally within each sector with the latitudinal average of the corresponding average of the total u^2 and v^2 derived from the upper left diagrams of Figs. 5 and 6. The mean of the five sectors is given as "N HEM" in Table 4.

Averaging over all sectors (i.e., "N HEM" in Table 4) the barotropic terms contribute 93 and 82 per cent of the total energy

Fig. 5. The breakdown of the u^2 component of specific kinetic energy into baroclinic, barotropic, transient, standing, eddy, and mean meridional components according to Eqn. (11). The terms are plotted by latitude for January 1964 and for the geographic sectors indicated in Table 1.

Fig. 6. The breakdown of the v'^2 component of specific kinetic energy into baroclinic, barotropic, transient, standing, eddy, and mean meridional components according to Eqn. (11). The terms are plotted by latitude for January 1964 and for the geographic sectors indicated in Table 1.

TABLE 4: Percentage contribution to $[u^2]_{(p,\lambda,t)}$ and $[v^2]_{(p,\lambda,t)}$ energy components by baroclinic, transient and eddy processes. The terms making up each of these classes are listed using the numbers in Eqn. (11)

SECTOR	NA		AO		E		A		PO		N HEM	
Class	u^2	v^2	u^2	v^2	u^2	v^2	u^2	v^2	u^2	v^2	u^2	v^2
baroclinic ②+④+⑥+⑧	6	16	6	12	9	10	8	20	6	19	7	18
barotropic ①+③+⑤+⑦	94	84	94	88	91	90	92	80	94	81	93	82
transient ⑤+⑥+⑦+⑧	14	79	24	74	23	63	10	76	12	82	16	75
standing ①+②+③+④	86	21	76	26	77	37	90	24	88	18	84	25
eddy ③+④+⑦+⑧	13	92	22	77	20	75	8	86	8	86	14	81
mean meridional ①+②+⑤+⑥	87	8	78	23	80	25	92	14	92	14	86	19

in the u- and v-components, respectively. Terms with "transient" and "eddy" characteristics provide 75 and 81 per cent of the energy in the v-component, respectively. This compares with 16 and 14 per cent of the energy contributed by these same terms to the u-component, demonstrating the larger variability with respect to time and longitude of the v-component (Kao and al-Gain, 1968; Wooldridge and Reiter, 1969).

The distribution with longitude of the "barotropic" (averaged over pressure $100 \leq p \leq 500$ mb) u- and v-components of kinetic

energy, averaged with respect to latitude (30^ON to 70^ON) and time
(1 to 30 January 1964) may be seen from Figs. 7 and 8. The peak
in the total barotropic kinetic energy, averaged in the same fashion,
that appears near 40^OE (bottom curve in Fig. 9) is to a large extent
caused by the $[v^2]_{(p,\phi,t)}$ contribution. This is in the region of the
European blocking high. Elsewhere--even on the west side of this
block over the Atlantic--the u-component dominates the total baro-
tropic kinetic energy distribution. The baroclinic contributions of
each pressure level are shown as functions of longitude in the upper
portions of Fig. 9. These contributions are defined as $[\frac{(u)^2_{(p)} + (v)^2_{(p)}}{2}]_{(\phi,t)}$.
As may be expected, the shears above and below the jet core, especially
near 100 and 500 mb, yield the largest values of this term. It is of inter-
est to note that the two jet stream regions over East Asia (100°-140^OE)
and over the eastern United States (80^OW) contribute mostly to the
"shear portion" of kinetic energy at the 500 and 200 mb levels. At
100 mb, however, a 3-wave pattern appears. Such a pattern, with
troughs near 60^OW, 40-60^OE and at 160^OE was actually present in the
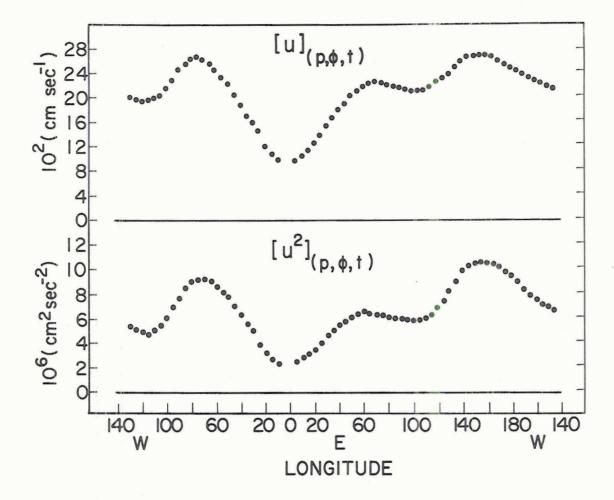stratosphere during part of the time period under consideration.

Fig. 7. Longitudinal distribution of $[u]_{(p,\phi,t)}$ and $[u^2]_{(p,\phi,t)}$ for the middle latitude upper troposphere during January 1964.
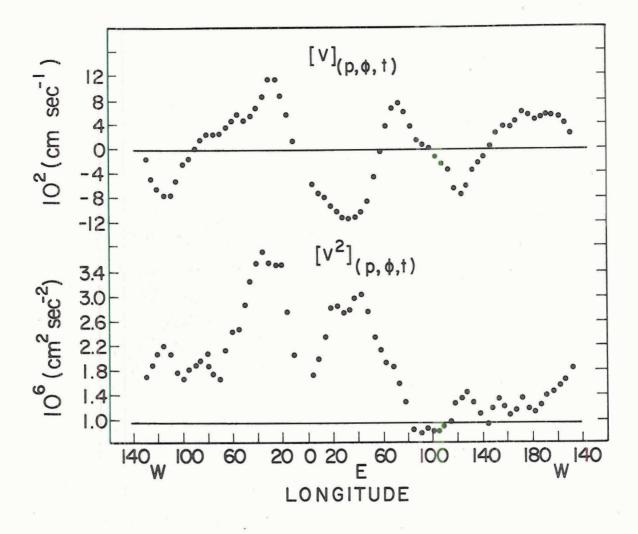
Fig. 8. Longitudinal distribution of $[v]_{(p,\phi,t)}$ and $[v^2]_{(p,\phi,t)}$ for the middle latitude upper troposphere during January 1964. Negative values indicate southward flow.
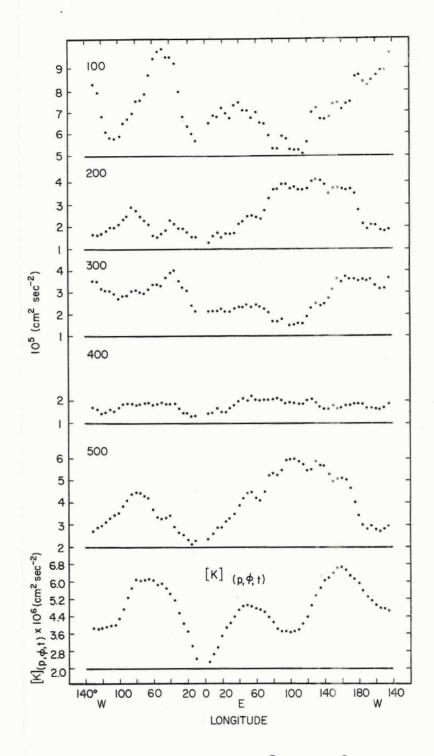
Fig. 9. Longitudinal variation of $[\{(u)^2_{(p)} + (v)^2_{(p)}\}/2]_{(\phi, \lambda)}$ for the pressure levels indicated in mb. The spatial averages are over the North American sector. The time average is over January 1964 (five upper curves). Lowest curve: The longitudinal variation of total kinetic energy, averaged over pressure and over the same coordinates as the upper curves.

8. Kinetic Energy and Radioactive Fallout

Cyclogenetic activity at the 300-mb level was estimated by computing Mahlman's (1966) cyclone index at this level along 50° lat and over the North American sector. This index is defined as

$$C = 1 - \frac{[\gamma^2]^{1/2}_{(\lambda)}}{90} \tag{13}$$

where γ is defined as "wind direction minus 270°". $C = 1.0$ for zonal flow, 0.0 for meridional flow. Mahlman found that cyclone index decreases $\frac{100(C_1 - C_2)}{\Delta t} > 2.5$ usually were accompanied by surface fallout events within five days from the time at which the observed decrease occurred. (Subscripts 1 and 2 refer to the beginning and end of the time period Δt.)

Computational results are shown in Fig. 10 (4th curve from top). Cyclone index decreases at 50°N agree well with the two major fallout events between 35° and 60°N and 60°-130°W (North America) (5th curve from top). Agreement is lacking, however, if one includes the fallout events north of 60°N (bottom curve in Fig. 10).

The upper 3 curves in Fig. 10 give the daily average values of the "shear", or baroclinic, contribution to kinetic energy $\frac{[(u)_{(p)} + (v)_{(p)}]_{(\lambda, \phi)}}{2}$ at 100, 300 and 500 mb for $60^\circ \leq \lambda \leq 130^\circ$W (North America) and $30^\circ \leq \phi \leq 70^\circ$N. Major peaks of "shear kinetic energy" precede the two major fallout events. These peaks occur in conjunction with cyclone index decreases, i.e., with flow turning into a meridional direction. The kinetic energy peaks signify strong vertical shears {large differences between $[u]_{(p)}$ and $u_{500\,mb}$ yielding large values of $(u)_{(500\,mb)}$} above the 500-mb level, as they are
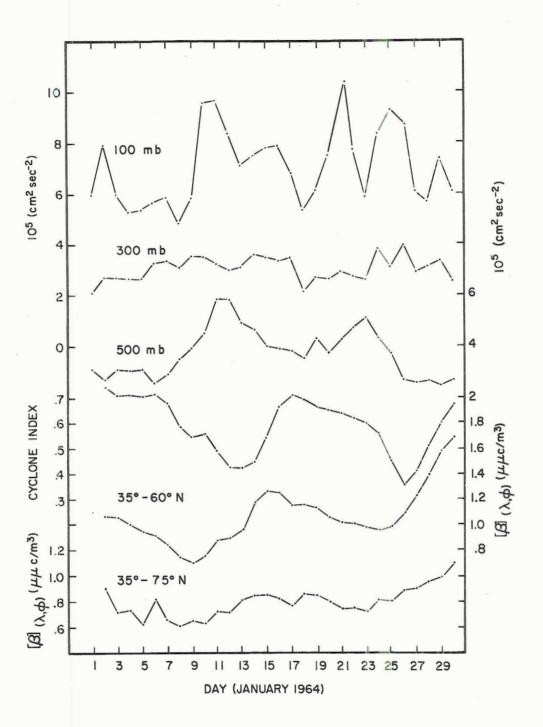
Fig. 10. Time variation of $[\{(u)^2_{(p)} + (v)^2_{(p)}\}/2]_{(\phi,\lambda)}$ for the North American sector and for the pressure levels indicated (three upper curves). Two lowest curves: The time variation of surface air β activity averaged over the North American sector between the latitudes indicated. The remaining curve gives the cyclone index for the North American sector computed for 50°N and at 300 mb.

expected to occur in the "jet stream front". The stable region of this frontal zone--from past synoptic experience--contains strato-spheric air contamined with radioactive debris.

The upper portion of Fig. 4 reveals more details of this "shear kinetic energy" at 500 mb over the North American sector as a func-tion of latitude and time. The north-to-south intrusions of strongly shearing jet streams, evidently possessing well developed baroclinic zones above 100 mb, may be seen on and after January 11 and 22. A less obvious "baroclinic intrusion" on January 19 near 45°N may well be linked to the minor fallout event on January 24. The fallout events at high latitudes obviously are not associated with mid-latitude baroclinic activity, as may be seen from Fig. 4.

9. Conclusions

    In the present study an attempt has been made to decompose total momentum flux and kinetic energy into 8 terms, signifying the contributions from barotropic, baroclinic, standing, transient, eddy, and mean meridional flow processes. The terms of Eqn. (11), with the exception of ① and ⑤ , differ from those derived by Starr and White (1951) and used by subsequent investigators. Due to limitations in computer memory (using a CDC 6400) hemispheric conditions were considered by comparing values in 5 sectors, each measuring 70° of longitude. This procedure provided limited insight into the behavior of the various flow processes in the low planetary-wave number regime.

    As is to be expected, southward momentum flux events in the middle latitude upper troposphere agree with radioactive fallout events at the earth's surface. Southward migration of areas with strong "shear kinetic energy" at the 500-mb level in middle latitudes also correlates well with major fallout events.

    For a prediction of such fallout events it appears, however, that Mahlman's (1966) cyclone index still holds the advantage of simplicity in its computation.

    The computational results presented in the foregoing chapters are only preliminary in nature. Further studies should include a comparison, on a hemispheric basis, of the 8 different terms of momentum flux and kinetic energy with the 4 terms derived by Starr and White (1951). A breakdown of the more important of the 8 terms in wave-number space (see e.g., Saltzman, 1957) is advocated. An inclusion of the lower troposphere into the treatment of "barotropic" and "baroclinic" flow process may also slightly modify the results

obtained above. Such extended computations would require either more elaborate programming techniques to extend the storage capabilities of the CDC 6400 presently available at Colorado State University or alternatively a larger computer facility.

Acknowledgements

References

Andrews, J. F., 1964: The weather and circulation of January 1964. Mon. Wea. Rev., Vol. 92, No. 4, pp. 189-194.

Barnes, A. A., Jr., 1962: Kinetic and potential energy between 100 mb and 10 mb during the first six months of the I. G. Y. Massachusetts Inst. of Tech., Dept. of Meteorology, Planetary Circulation Project, Final Report.

Danielsen, E. F., 1959: A determination of the mass transported from stratosphere to troposphere over North America during a thirty-six hour interval (abstract). Mitteilungen des Deutschen Wetterdienstes, Vol. 20, pp. 10-11.

_____, 1964: Project Springfield Report. Defense Atomic Support Agency, 99 pp.

Jensen, C. E., 1961: Energy transformation and vertical flux processes over the Northern Hemisphere. J. Geophys. Res., Vol. 66, No. 4, pp. 1145-1156.

Kao, S.-K., and A. A. al-Gain, 1968: Large-scale dispersion of clusters of particles in the atmosphere. J. Atmos. Sci., Vol. 25, No. 2, pp. 214-221.

Mahlman, J. D., 1964: Relation of stratospheric-tropospheric mass exchange mechanisms to surface radioactivity peaks. M. S. Thesis, Colorado State University, 54 pp.

_____, 1965: Relation of tropopause-level index changes to radioactive fallout fluctuations. Atmos. Science Paper No. 70, Colorado State Univ., pp. 84-109.

_____, 1966: Atmospheric general circulation and transport of radioactive debris. Atmos. Science Paper No. 103, Colorado State Univ., 184 pp.

Miller, A. J., S. Teweles, and H. M. Woolf, 1967: Seasonal variation of angular momentum transport at 500 mb. Mon. Wea. Rev., Vol. 95, No. 7, pp. 427-439.

Murray, F. W., 1963: Computer applications in stratospheric analysis and forecasting. Seminars on the Stratosphere and Mesosphere and Polar Meteorology (F. K. Hare, editor), Publication in Meteorology No. 65, Arctic Meteorology Research Group, Department of Meteorology, McGill University (Scientific Report No. 9, AF 19(604)-8321, AFCRL-64-197, pp. 69-81.

Oort, A. H., 1964: On estimates of the atmospheric energy cycle. Mon. Wea. Rev., Vol. 92, No. 11, pp. 483-493.

Reiter, E. R., 1963a: Jet Stream Meteorology. University of Chicago Press, 513 pp.

_____, 1963b: A case study of radioactive fallout. J. of Appl. Meteor., Vol. 2, pp. 691-705.

_____, 1969a: Atmospheric transport processes, Part I: Energy transfers and transformations. AEC Critical Review Series (in print).

_____, 1969b: Mean and eddy motions in the atmosphere. Mon. Wea. Rev., Vol. 97, No. 3, pp. 200-204.

_____, M. E. Glasser, and J. D. Mahlman, 1967: The role of the tropopause in stratospheric-tropospheric exchange processes. Atmos. Science Paper No. 107, Colorado State Univ., 80 pp.

_____, _____, and _____, 1969: The role of the tropopause in stratospheric-tropospheric exchange processes. Pure and Applied Geophys. (to be published).

_____, and J. D. Mahlman, 1964: Heavy radioactive fallout over the southern United States, November 1962. Atmos. Science Paper No. 58, Colorado State Univ., pp. 21-49.

_____, and _____, 1965: Heavy radioactive fallout over the southern United States, November 1962. J. Geophys. Res., Vol. 70, pp. 4501-4520.

Saltzman, B., 1957: Equations governing the energetics of the larger scales of atmospheric turbulence in the domain of wave number. J. Meteor., Vol. 14, No. 6, pp. 513-523.

Sawyer, J. S., 1965: Notes on the possible physical causes of long-term weather anomalies. WMO Technical Note, No. 66, World Meteorological Organization, pp. 227-248.

Starr, V. P., and R. M. White, 1951: A hemispherical study of the atmospheric angular momentum balance. Q. J. Roy. Meteor. Soc., Vol. 77, No. 332, pp. 215-225.

Wooldridge, G., and E. R. Reiter, 1969: Large scale atmospheric circulation characteristics as evident from GHOST balloon data; (Presented at the Conference on the Global Circulation of the Atmosphere, London, August, 1969).